DEVELOPMENT AND VALIDATION OF A LIGHTWEIGHT PHYSICS-BASED INDOOR CELLULAR PROPAGATION SIMULATOR

Hyundeok Choi
Wayland Academy
Beaver Dam, United States of America
ceramiccreativing@gmail.com

***Abstract*—Cellular calls and mobile data became unstable at locations in the author's dormitory while outdoor signal remained strong. It was hypothesized that indoor cellular signal strength could be simulated with useful accuracy using a lightweight model utilizing extended high school physics equations without an electromagnetic simulator. To test this hypothesis, the author developed an indoor cellular propagation simulator using ray tracing and extended high school physics equations. The program converted the dorm floor plan into a calculation grid and modeled distance loss and material-crossing loss. Building materials were identified with dormitory supervisors' assistance, and the floor plan was measured and modeled with Blender and Free CAD. Signal strength was measured five times at nine indoor and two outdoor locations with the same handset, carrier, and SIM. For validation, the measurements were compared with calculations from the program and reference results from an electromagnetic simulator. The program produced a mean absolute error (MAE) of 6.57 dB, versus 7.78 dB for the simulator, and placed the two weakest measured locations among its three lowest estimates. These results suggest that extended high school physics can simulate indoor cellular propagation with useful accuracy and assist students in identifying weak-reception areas within dormitories**

Keywords— Engineering, Electrical Engineering, Path Loss Modeling, Ray-Tracing Based Propagation Modeling, Indoor Cellular Propagation Simulation

I. INTRODUCTION

In the author's dormitory, a phone could maintain a reliable connection near a window, yet calls and mobile data often became unstable only a few meters farther inside. Similar reception problems were observed in several other indoor environments in suburban towns. For students who rely on mobile networks to access information or make emergency calls, these coverage gaps are a practical concern. Distance alone, however, cannot fully explain such uneven reception. Building materials, interior layouts, and multipath propagation also influence how signals travel through a building. One measure commonly used in handset-based field assessments is reference signal received power (RSRP), which represents the received power of cell-specific LTE reference-signal resource elements.[1] Several approaches can be used to predict indoor signal strength. Log-distance and multi-wall models provide relatively simple estimates,[2] whereas more detailed deterministic methods trace propagation mechanisms such as reflection, transmission, and diffraction.[3-4] ITU-R P.1238 describes how propagation varies with distance inside buildings and provides guidance for planning indoor radiocommunication systems.[5] Earlier measurement-based studies further demonstrate why distance must be considered together with the physical features of a building. For example, Seidel and Rappaport incorporated partitions, concrete walls, floors, and building layout, in addition to distance, into their site-specific 914 MHz models. Across the complete dataset, the standard deviation between measured and predicted path loss was 5.8 dB.[6] Plets *et al*. later used free-space loss as the basis of a simple heuristic algorithm for predicting indoor coverage. Validation measurements collected across multiple floors of four buildings showed close agreement with their predictions.[7] Hossain *et al*. examined indoor propagation at the higher frequency of 28 GHz. They validated an efficient three-dimensional ray-tracing method by comparing simulated received signal strength and path loss with measured values.[8] Together, these studies show that both relatively simple models and methods that represent propagation geometry in greater detail have been used to predict indoor coverage. The purpose of this study was to evaluate how accurately a student-developed lightweight model could reproduce measured indoor Band 66 signal-strength patterns and to compare its performance with that of the more physically detailed Ansys HFSS SBR+ model. The lightweight model applied concepts from high-school physics, particularly those taught in AP Physics 2, to indoor cellular propagation. Four questions guided the evaluation. How closely did the model's predictions match the measured Band 66 signal strength? Could the model identify weak-signal locations within the dormitory? How did its predictions compare with those produced by Ansys HFSS SBR+? Finally, which building features and model limitations were associated with large prediction errors? The study hypothesized that a lightweight model based on high-school physics equations could achieve useful accuracy by accounting for distance loss and the material-crossing losses associated with walls, doors, windows, and other interior structures. Specifically, the model was expected to reproduce the overall indoor cellular signal distribution and identify the main weak-signal locations. However, only one lightweight model was tested, and individual propagation mechanisms were not added or removed in separate tests. The study therefore could not determine which mechanisms were essential for accurate simulation. Its conclusions were limited to the performance of this particular model,

including how accurately it predicted signal strength, where it performed well, and where substantial errors occurred.

II. Methods

A. Study site and measurement area

The study was conducted on the fourth floor of Wayland Hall in the United States. The study area measured approximately 34.0 m by 18.4 m and contained dormitory rooms, corridors, windows, structures, and interior and exterior walls. The scope focused on locations where the author experienced unstable cellular connectivity during ordinary residence in the 2025-2026 academic year. A digital model was constructed in Blender and Free CAD from field dimensions and existing drawings.[9] Building materials such as brick, glass, and wood were distinguished, whereas door frames, window frames, furniture details, and the interior structure of the rooms, excluding the author's room, were simplified to reduce computational complexity. The lightweight model and Ansys SBR+ used the same base floor plan and simplifications. The three-dimensional computer-aided design (CAD) model, the fourth-floor digital twin, and the field-validation locations are shown in Figures 1–3, respectively.

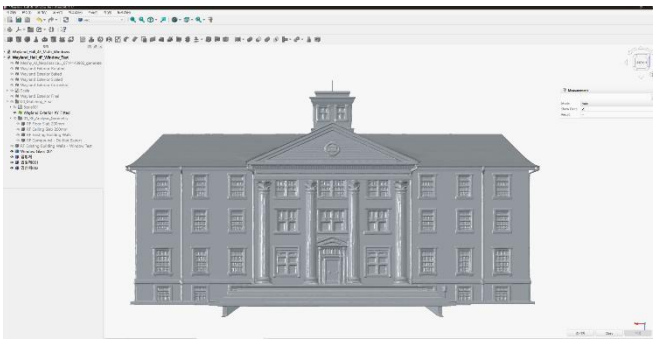

Figure 1. Three-dimensional computer-aided design (CAD) model of Wayland Hall used to represent the building geometry in the propagation simulations. The initial exterior geometry was generated using Meshy AI (https://www.meshy.ai/) and was subsequently imported, scaled, corrected, and edited by the author using Free CAD 1.1.1.

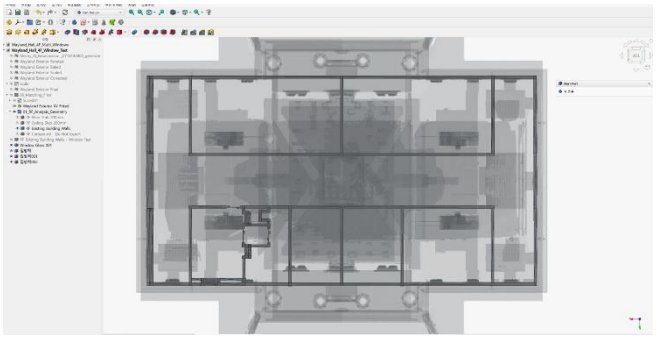

Figure 2. Fourth-floor digital twin of Wayland Hall showing the interior geometry used as the basis for both propagation simulations. The digital twin was constructed and edited by the author using Blender 5.1 (Blender 5.1: https://www.blender.org/) to process the mesh geometry and Free CAD 1.1.1 to convert the mesh geometry into solid bodies using the Part Workbench and correct the model.

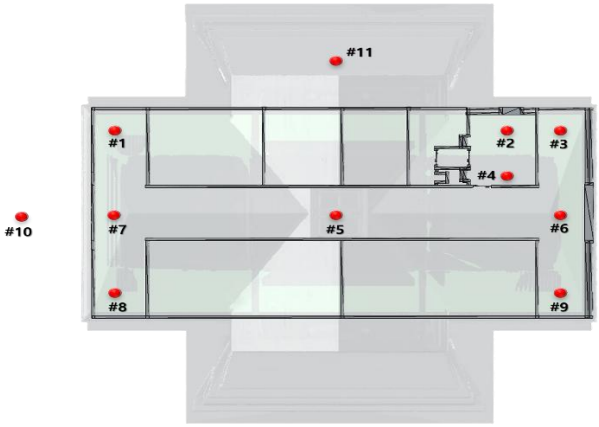

Figure 3. Fourth-floor field-validation layout showing nine indoor measurement locations (1–9) and two outdoor reference locations (10 and 11) used to compare measured and simulated reference signal received power (RSRP). The layout and location labels were prepared by the author using Free CAD 1.1.1 and Microsoft PowerPoint for Microsoft 365, version 2508. (https://www.microsoft.com/microsoft-365/powerpoint).

B. Outdoor survey and band selection

Preliminary outdoor measurements were taken at points #10 and #11. Point #10 predominantly received Band 13 from Cell ID 53636610. Because that cell was rarely observed indoors, point #10 was excluded from the Band 66 analysis. At point #11, Band 66 from Cell ID 53636630 was received consistently, and the same Cell ID was detected at several indoor points. The Band 66 signal was therefore assumed to enter primarily from the north side of the building, and the following conditions were applied to both analyses shown in Figure 4:

- Band: Band 66
- Center frequency: 2.155 GHz
- Reference Cell ID: 53636630
- Incidence direction: North
- Outdoor reference point: #11
- Reference RSRP: -93 dBm

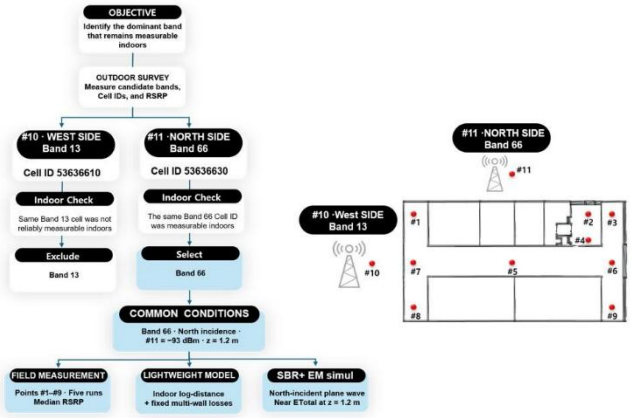

Figure 4. Band-selection and validation workflow (left) and measurement locations with reference-signal directions (right). The diagram was created by the author using Microsoft PowerPoint based on field records and the study geometry; RSRP denotes reference signal received power, Cell ID denotes cell identifier, and SBR+ denotes shooting and bouncing rays.

C. Measurement points and coordinates

The indoor validation set consisted of points #1 to #9. Point #10 was excluded, and point #11 served as the Band 66 reference. All measurements and simulation outputs were evaluated 1.2 m above the floor shown in Table 1.

Table 1. Coordinates and location descriptions of the nine indoor validation points used to compare measured and simulated reference signal received power (RSRP). The x-coordinates and y-coordinates are reported relative to the floor-plan origin, and z represents the measurement height above the floor, fixed at 1.2 m for all points.

Point	Position	X (m)	Y (m)	Z (m)
#1	Northwest room	1.6	17.4	1.2
#2	Interior northeast room	28.5	17.4	1.2
#3	Far northeast room	31.8	17.4	1.2
#4	Upper east corridor	28.5	12.7	1.2
#5	Central corridor	15.9	9.2	1.2
#6	Central east corridor	31.8	9.2	1.2
#7	Central west corridor	1.6	9.0	1.2
#8	Southwest room	1.6	1.6	1.2
#9	Southeast room	31.8	1.6	1.2

D. Repeated indoor field measurements

Measurements were collected from May 11 to May 17, 2026, using Field Test Mode on the same iPhone 17 Pro, carrier, and SIM. The primary collection was completed on May 16. Band, Cell ID (Cell Identifier), and reference signal received power (RSRP) were recorded at indoor points #1 to #9 and outdoor reference point #11 during five complete runs with approximately 30 minutes between repeated readings at the same point. The handset was held at a height of 1.2 m, room doors remained closed, and no other people were present in the measurement area. Tests conducted with the handset facing east, west, south, and north showed RSRP differences of approximately 1 dB or less. The median of the five readings was used as the representative value at each point. The complete measurement conditions are given in Table 2.

Table 2. Configuration and controlled conditions for repeated long-term evolution (LTE) field measurements at nine indoor validation points (#1 to #9) and outdoor reference point #11. The same handset, subscriber identity module (SIM), serving cell, measurement height, and environmental conditions were maintained across all sessions; RSRP denotes reference signal received power, PCI denotes physical cell identity, TAC denotes tracking area code, Cell ID (cell identifier) denotes cell identifier, PLMN denotes public land mobile network, and z denotes height above the floor.

Item	Value
Handset	Apple iPhone 17 Pro (same unit for all five runs)
Measurement tool	Apple iOS Field Test Mode (iOS version not recorded); LTE serving cell parameters
Carrier	Visible (Verizon network)
Frequency	Band 66 downlink; 2.155 GHz center; 10 MHz bandwidth
Serving cell	PCI 313; TAC 53536; Cell ID 53636630; PLMN 311 480
Measurements height	z = 1.2 m (fixed)
Repeats	Five readings per point
Representative value	Median of five readings
Measurement period	May 11-17, 2026; 8:00-10:00 p.m.

RSRP was selected as the primary evaluation metric because it quantifies the received power of LTE reference signals and supports direct comparison of propagation attenuation across locations and building features.[1,10]

E. Lightweight propagation model

For this study, the author developed a lightweight propagation model using a two-dimensional direct-path multi-wall approach.[2,6] The calculation used a fixed reference of −93 dBm, taken from the Band 66 RSRP measurement at point #11. This value was assigned to the north-side incidence boundary for comparison with the field measurements and Ansys SBR+ results. For each measurement point, the program traced a direct path from the boundary and identified the structures along it. The indoor distance loss and the losses from crossing these structures were then summed and subtracted from the reference level to estimate RSRP. Users could set the incidence direction to north, south, east, or west and check the predicted signal strength at a location of their choice. Selected walls, windows, and wooden structures in the fourth-floor Wayland Hall model could also be added or removed individually. This allowed users to examine how changes to the building affected the predictions. For the quantitative comparison reported here, only north-side incidence and the existing building configuration were used (Figures 5–6). Multiple reflections, diffraction, and phase interference were not explicitly calculated, which reduced computational complexity. With these simplifications, the program operated as a reduced-complexity propagation model rather than a conventional electromagnetic ray-tracing solver. Figure 5 shows the building configuration before simulation. An example of the calculation at an individual point is presented in Figure 6.

Figure 5. The pre-simulation geometry-configuration interface of the author-developed lightweight propagation model shows the fourth-floor layout of Wayland Hall, indoor measurement points MP01 to MP09, or #1 to #9, and the structure type, material, thickness, and segment settings used to construct and modify the two-dimensional propagation geometry. The screenshot was captured by the author from the self-developed Wayland Signal Quest lightweight simulation.

Figure 6. The point-by-point calculation carried out by the author using their own lightweight propagation model for indoor measurement point 5 (MP05) when subjected to north-side Band 66 incidence at a frequency of 2.155 GHz showed that, with a RSRP (reference signal received power) of −93 dBm at point #11, the model determined a distance loss of 19.3 dB and a structure-crossing loss of 14.0 dB, which resulted in a total indoor loss of 33.3 dB and an estimated RSRP of −126.3 dBm for a direct-path distance of 9.2 m. The screenshot was obtained by the author from the author's Wayland Signal Quest lightweight simulation.

F. Reference RSRP and Relative Attenuation Calculation

To compare the field measurements with the outputs of the lightweight model and Ansys SBR+ on a common basis, the measured Band 66 RSRP at north-side outdoor reference point #11 (−93 dBm) was used as the reference RSRP. Point #11 was used only to define the reference signal level and was not treated as the physical signal source in either model. The lightweight-model paths originated at the north-side building boundary, while SBR+ used a plane wave incident from the north. The base-station location and transmit power were not modeled directly. Instead, propagation from the base station to point #11 was treated as a common baseline, and the attenuation at each indoor point was calculated relative to this reference:

$$Lmeas,i = RSRPref - RSRPmeas$$

$Lmeas,i$ = measured relative attenuation at a variable point i (dB).

$RSRPref$ = measured RSRP at reference point #11 (-93 dBm).

$RSRPmeas$ = median measured RSRP at a variable point i (dBm).

An identical reference-based calculation was carried out separately for both the lightweight-model and the SBR+ estimates at point i. Hence the obtained values indicate attenuation in comparison with point #11 and not the total path loss from the base station. The boundary reference and incidence direction were chosen so that the lightweight model would correspond with the north-side incident plane-wave setup used in Ansys SBR+.[11] This decision set a common reference for the incident signal when carrying out the comparison; the distance-loss exponent remained a separate assumption, as explained below.

G. Indoor distance loss

Indoor distance loss in the lightweight model was calculated with the log-distance path-loss equation:

$$L\,d,i \;=\; 10n\,log(\frac{di}{do})$$

n: path-loss exponent, set to 2 in this study.

The distance power-loss coefficient stated in ITU-R P.1238-13 is about 20 for paths which have a line-of-sight component and for large open rooms, especially in the 900–2,000 MHz range.[5] In the notation employed here, this coefficient is equivalent to n = 2 and thus serves as a baseline similar to that of free space.[12]

di: distance from the reference boundary to receiving point i.

do: reference distance, set to 1 m; additional loss beyond 1 m was calculated logarithmically

Because the additional losses caused by walls, doors, and windows were calculated separately, n = 2 was adopted as a literature-based default for the distance term.[7] This separated the baseline distance attenuation from the structure-crossing losses and kept the model simple. Applying this term to distance measured from the building boundary, rather than from the physical transmitter, was an approximation adopted in this study. Thus, the boundary reference and incidence direction were matched to the Ansys plane-wave configuration, whereas n = 2 was a separate assumption of the lightweight model and was not derived from the plane-wave excitation itself.

H. Structure-crossing loss

Indoor propagation experiences additional loss as a signal crosses walls, doors, and windows. ITU-R P.2040 indicates that transmission through building materials varies with material and frequency.[13] Measurements reported in NISTIR 6055 were also consulted.[14] The representative crossing-loss coefficients in Table 3 were applied at Band 66 (2.155 GHz). There is a precedent for using representative penetration losses in simplified indoor propagation models: in Section 5.2 of Plets *et al.*, measurements were made of the losses for some types of wall, while for other materials the losses were obtained from the published literature; distinction was also made between thin and thick walls.[7] This offers a methodological basis for making use of losses derived from the literature when detailed measurements of each building component are not available, even though it does not specify the coefficients that were used in the present study. The values for the brick, wood, and glass coefficients given in Table 3 were taken as representative figures for the simplified building model, based on the

available data regarding the materials and the thicknesses of these materials. These values indicate the amount of attenuation associated with one pass through a component and were not determined separately in Wayland Hall. Although NISTIR 6055 includes measurements of attenuation as a function of material, thickness, and frequency, the measurement bands listed are 0.5–2 GHz and 3–8 GHz.[14] Accordingly, the use of this document here allows for an approximate choice of the attenuation values rather than representing a direct measurement at 2.155 GHz. The values selected are based on model assumptions and are not universal constants for these materials. The representative material crossing-loss coefficients used for the lightweight model at Band 66 (2.155 GHz) were chosen by the author in accordance with ITU-R P.2040 and NISTIR 6055; these are approximate losses per component crossing and not the actual measured losses of the individual walls, doors, or windows in Wayland Hall.[13-14]

Table 3. Representative material crossing-loss coefficients adopted for the lightweight model at Band 66 (2.155 GHz). The coefficients were selected by the author with reference to ITU-R P.2040 and NISTIR 6055; they are approximate losses per component crossing, not measured losses of the individual walls, doors, or windows in Wayland Hall.[13-14]

Material	Band 66 crossing-loss coefficient	Places that are applied to
Brick	10.0 dB/crossing	Interior and exterior walls
Wood	3.5 dB/crossing	Interior doors
Glass	4.0 dB/crossing	Windows

Structure loss was calculated from the types and numbers of structures intersected by the direct path. The total structure-crossing loss was calculated as follows:

$$Lmat, i \;=\; \Sigma k\; Ni, k \;\times Lk$$

$Lmat, i$= total structure-crossing loss to variable receiving point i (dB).

Ni, k= number of times the path to variable point i crosses material k.

Lk= loss for one crossing of material k (dB).

I. Ansys HFSS SBR+ comparison simulation

The building materials were represented using nominal thicknesses and representative electrical properties informed by available information about the building components. These inputs were idealizations of the actual construction. ITU-R P.2040-4 provides a methodological basis for such material representations: Section 3 and Table 3 give representative, frequency-dependent permittivity and conductivity models derived from published measurements, and Section 2.1.2.4 relates these quantities to the dielectric loss tangent.[13] This supports the use of representative material properties for propagation modeling, but does not establish a universal wall thickness or a fixed loss per crossing. Ansys HFSS SBR+ was used as the commercial electromagnetic analysis reference employed for comparison with the lightweight model.[15] Ansys provided the reference results using version 2026 R1.2; the author used the Academy version 2025 R2. SBR+ is a high-frequency asymptotic shooting-and-bouncing-ray method that is designed for the efficient calculation of propagation and scattering in electrically large structures; however, the SBR+ algorithm was not developed in the present study.[16] In order to ensure comparable conditions, the SBR+ model used 2.155 GHz (Band 66), north-side incidence, and the same simplified fourth-floor Wayland Hall geometry. A plane wave was made to impinge from the north, and the near-field distribution was computed on a plane located 1.2 m above the floor, at the measurement height, as illustrated in Figure 7. Ansys HFSS SBR+ has the capability of carrying out near-field analysis with an incident plane wave.[11] The SBR+ result was exported in the form of dB (NearETotal). This quantity was not the cellular RSRP; it was the total electric-field magnitude calculated by SBR+ and given in decibels. For this electric-field quantity, the Ansys dB function is defined below using a base-10 logarithm.[17]

$$Ed\ B, i \;=\; 20log10|Ei|$$

$Ed\ B, i$: electric-field magnitude at analysis point i (dB)

Ei: NearETotal electric-field magnitude at analysis point i.

For comparison with measured RSRP, the electric field at each point was normalized to the reference electric field, $Eref$:

$$\Delta Ei \;=\; 20log10(\frac{|Ei|}{|Eref|})$$

ΔEi: change in electric-field magnitude at point i relative to the reference (dB).

$Eref$: electric-field magnitude at the reference location.

Ei: electric-field magnitude at analysis point i.

The normalized relative electric-field values were aligned with the measured reference RSRP at point #11 to produce an RSRP-equivalent value for comparison:

$$RSRP\ SBR, i = \;RSRPref \;+\; \Delta Ei$$

Because the Band 66 reference RSRP at point #11 was -93 dBm in this study,

$$RSRP\ SBR, i = \;-93 + \;\Delta Ei$$

$RSRP\ SBR, i$: RSRP-equivalent comparison value obtained by aligning the relative SBR+ field with the measured reference signal (dBm).

$RSRPref$: measured Band 66 RSRP at reference point #11 (-93 dBm).

Thus, $RSRP\ SBR, i$ was not an $RSRP$ value calculated directly by SBR+. It was a comparison value produced by normalizing the relative SBR+ electric-field distribution to the measured reference signal. NearETotal values at the same coordinates as measurement points #1 to #9 were extracted and compared with the lightweight-model estimates and field measurements.

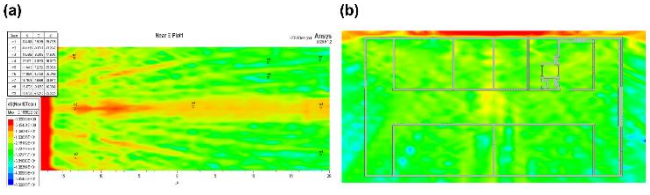

Figure 7. The simulated near-field electric-field distribution on the fourth floor of Wayland Hall at a frequency of 2.155 GHz with a plane wave incident from the north side, as evaluated at a height of 1.2 m above the floor, is as follows: (a) a field map which includes sampling markers and a color scale indicating the magnitude of the electric field in decibels, dB (NearETotal); (b) the same distribution with the floor plan geometry superimposed. The reference panels were provided by Ansys (version 2026 R1.2) through Taehyung Kim, the study mentor; the author used the Academy version 2025 R2.

J. Common analysis conditions and comparison basis

The common conditions listed in Table 4 were applied so that the lightweight-model and Ansys HFSS SBR+ outputs could be compared under the same experimental configuration.

Table 4. Common conditions used to compare the lightweight propagation model with the Ansys HFSS shooting and bouncing rays (SBR+) simulation. The frequency, incident-wave direction, reference RSRP (reference signal received power), evaluation points, building geometry, and material configuration were defined by the author and applied consistently to both models.

Item	Condition
Frequency	Band 66 receive frequency (2.155 GHz)
Incident-wave direction	North-side incidence
Reference source	Outdoor point #11; -93 dBm
Evaluation points	Nine indoor points (#1-#9; #10 is excluded)
Spatial basis	Same fourth-floor floor plan and structural layout, represented in two dimensions by the lightweight model and three dimensions by SBR+
Evaluation height	1.2 m above the fourth-floor level
Materials	Exterior walls, interior walls, windows, and wooden interior doors

Although both models were based on the same fourth-floor layout and assumed that the signal entered from the north, they represented the building and calculated signal propagation differently. The lightweight model treated the building as a two-dimensional floor plan and estimated RSRP by combining direct-path distance loss with structure-crossing loss. SBR+, in comparison, used a three-dimensional model developed from the same floor plan and a commercial electromagnetic solver to calculate the spatial electric-field distribution. Accordingly, the study did not attempt to make the two methods identical. Instead, it evaluated how closely each model reproduced the measured RSRP under the same experimental conditions. The two models also showed material effects at various levels of detail; SBR+ employed the assumed geometry and electromagnetic material properties, while the lightweight model assigned a fixed loss for each material crossing. Since they shared the same material classification, this does not mean that the transmission losses are the same in the two models. In the case of the lightweight model, the thickness variations within each material category were not taken into account by the fixed coefficients given in Table 3.

K. Comparison of measured and simulated values

The following three values were compared at the same coordinates for indoor points #1 to #9:

- Median RSRP from five repeated measurements
- RSRP estimated by the lightweight propagation model
- Normalized RSRP-equivalent value from Ansys HFSS SBR+

$$ei = RSRPpred,i - RSRPmeas,i$$

ei: signed prediction error at point i (dB).

$RSRPpred,i$: lightweight-model or SBR+ estimate at point i (dBm).

$RSRPmeas,i$: measured median RSRP at point i (dBm).

The magnitude of the error at each point was calculated as an absolute error:

$$A\,Ei = |ei|$$

$A\,Ei$: absolute error at point i (dB).

L. Model-accuracy evaluation

Overall accuracy for the lightweight model and SBR+ was evaluated across indoor points #1 to #9 using mean absolute error (MAE) and root mean square error (RMSE):

$$MAE = \frac{1}{N}\sum_{i=1}^{N}|ei|$$

$$RMSE = \sqrt{\frac{1}{N}\sum_{i=1}^{N}ei^2}$$

ei: signed prediction error at point i (dB).

N: number of indoor validation points.

MAE: Mean Absolute Error across all validation points (dB).

$RMSE$: Root Mean Square Error, which weights larger errors more strongly (dB).

Since MAE and $RMSE$ involve calculating the difference between the predicted and the actual values, smaller values show that there is closer agreement between the simulations and the measured $RSRP$. The prediction error at each location was determined by comparing the measured median $RSRP$ with the output from each of the models. The errors obtained at each individual location were then employed to compute the overall MAE and $RMSE$ for the nine indoor validation points. The author carried out all the calculations using the figures given in Table 5.

III. Results and Discussion

A. Measured RSRP

At the indoor validation locations numbered #1 to #9, the medians from five repeated RSRP measurements varied between -106 and -123 dBm. The interquartile ranges were between 0 and 9 dB, with the smallest amount of variability being recorded at point #7 and the highest at point #8 (Figure 8). Figure 9 provides a visual comparison of the measurement configuration and the different representations of indoor propagation produced by the lightweight model and SBR+.

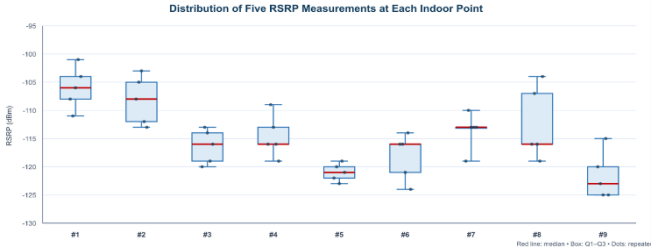

Figure 8. Distribution of five reference signal received power (RSRP) measurements taken at each of the indoor validation points (#1 to #9): the red

lines represent the medians, the boxes display the first and third quartiles, and the whiskers indicate the observed ranges; the median RSRP values varied from −106 to −123 dBm, the highest variation occurring at point #8. The graph was created by the author from field measurements using Microsoft Excel, version 16.0 (https://www.microsoft.com/microsoft-365/excel).

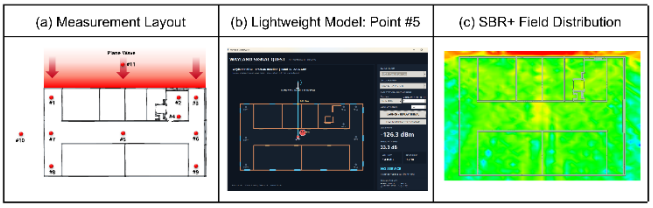

Figure 9. A comparison of the measurement layout and the results of the modeled indoor propagation under the same Band 66 conditions: panel (a) displays the indoor validation points #1 to #9 and reference point #11 on the north side which were used for the field measurements; panel (b) gives an example of the point-specific RSRP (reference signal received power) calculation carried out by the two-dimensional lightweight model at point #5; panel (c) shows the dB(NearETotal, or total near-field electric-field magnitude) distribution calculated by the three-dimensional Ansys HFSS SBR+ (shooting and bouncing rays) model, from which the normalized RSRP-equivalent values were obtained; even though the models have different dimensions and produce different output quantities, the three panels illustrate how each method represents the propagation throughout the same fourth-floor layout with signal incidence from the north side. The author assembled the figure in Microsoft PowerPoint for Microsoft 365, version 2508, using the field-measurement layout, outputs from the author-developed Wayland Signal Quest simulator, and Ansys-provided HFSS SBR+ reference results (2026 R1.2).

Table 5. Measured median reference signal received power (RSRP), the predictions from the lightweight model, and the normalized Ansys HFSS shooting and bouncing rays (SBR+) RSRP (reference signal received power)-equivalent values are compared point by point, together with the absolute error (AE) for indoor validation points #1 to #9. The lightweight model showed a smaller AE at points #4 through #9, while SBR+ had the smaller absolute error at points #1 to #3; all the values were calculated by the author using the field measurements and the model outputs.

Point	Measured Median (dBm)	Lightweight model (dBm)	Absolute Error (dB)	SBR+ equivalent RSRP (dBm)	Absolute Error (dB)
#1	-106	-97.0	9	-114	8
#2	-108	-97.0	11	-107	1
#3	-116	-97.0	19	-112	4
#4	-116	-112.0	4	-110	6
#5	-121	-126.3	5.3	-130	9
#6	-116	-116.3	0.3	-130	14
#7	-113	-116.5	3.5	-128	15
#8	-116	-121.5	5.5	-110	6
#9	-123	-121.5	1.5	-130	7

The measured value of RSRP was lowest at point #9 (−123 dBm), followed by point #5 (−121 dBm). The lightweight model produced its lowest estimate at point #5 (−126.3 dBm), followed by equal estimates at points #8 and #9 (−121.5 dBm). The model thus partly correctly identified the locations of the weak signals, since points #5 and #9 were among the ones with the lowest estimates, but it did not reproduce the exact measured ranking of these points because it also predicted a similarly weak signal at point #8. The lightweight model was nearer to the measured values than SBR+ at six points (points #4 to #9), while SBR+ had the smaller error at three points (points #1 to #3) (Table 5).

B. Overall model accuracy

Accuracy across validation points #1 to #9 was compared using MAE and RMSE (Table 6).

Table 6. Overall comparison of the lightweight propagation model and Ansys HFSS shooting and bouncing rays (SBR+) at the indoor validation points #1 to #9, using mean absolute error (MAE), which indicates the average error magnitude; root mean square error (RMSE),or accuracy metrics, which places more weight on larger errors; and maximum absolute error (AE), which shows the biggest error at a single point. The lightweight model had slightly smaller MAE and RMSE, while SBR+ had the lower maximum AE; all the values were calculated by the author from the point-by-point errors given in Table 5.

Metric	Lightweight Model	Ansys SBR+
MAE	6.57 dB	7.78 dB
RMSE	8.51 dB	8.84 dB
Maximum AE	19.0 dB	15.0 dB

At the nine indoor validation points, the lightweight model showed an MAE of 6.57 dB and an RMSE of 8.51 dB; the magnitude of its pointwise absolute errors varied between 0.3 and 19.0 dB. SBR+ achieved an MAE of 7.78 dB and an RMSE of 8.84 dB, indicating that the two models differed by 1.21 dB in MAE and by 0.33 dB in RMSE. Nevertheless, the largest absolute error for the lightweight model was 19.0 dB at point #3, as against 15.0 dB for SBR+. These results demonstrate that the two models had similar overall error magnitudes under the tested conditions, but neither of them was consistently more accurate at all locations.

C. Location-dependent error

Prediction accuracy varied across the floor. At the northern validation points #1 to #3, the lightweight model predicted signal strengths 9–19 dB above the measured values. SBR+ was closer to the measurements at all three points (Figures 10 and 11). The largest error in the lightweight predictions occurred at point #3. At points #4 to #9, however, the lightweight model performed better than SBR+ at every location, with absolute errors ranging from 0.3 to 5.5 dB. At point #6, for example, its error was 0.3 dB, compared with 14 dB for SBR+. The largest errors in the lightweight predictions occurred in the northern part of the floor, near the assumed north-side incidence boundary. The model's simplified treatment of signal entry through exterior structures may have contributed, along with uncertainty in the material-loss coefficients and room geometry. Reflection, diffraction, multipath propagation, and angle-of-incidence effects were also excluded from the calculations and may have influenced the results. These remain possible explanations, however, because the study did not test the factors individually and could not establish which were responsible for the large errors at these locations.

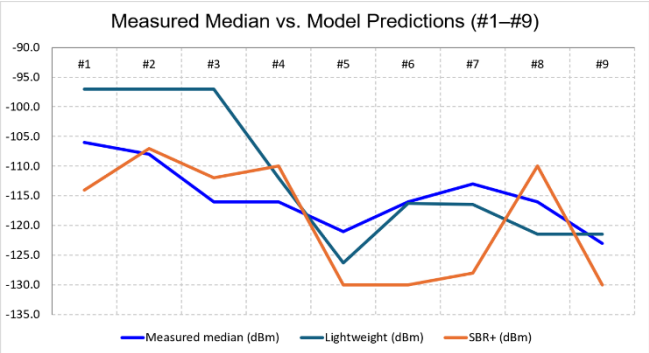

Figure 10. Comparison of median measured RSRP (reference signal received power), the estimates from the lightweight model, and the normalized Ansys HFSS shooting and bouncing rays (SBR+) RSRP-equivalent values at indoor validation points #1 to #9; the lightweight model was closer to the measured values at points #4 through #9, while SBR+ was closer at points #1 to #3; the graph was prepared by the author using field measurements and model outputs using Microsoft Excel, version 16.0.

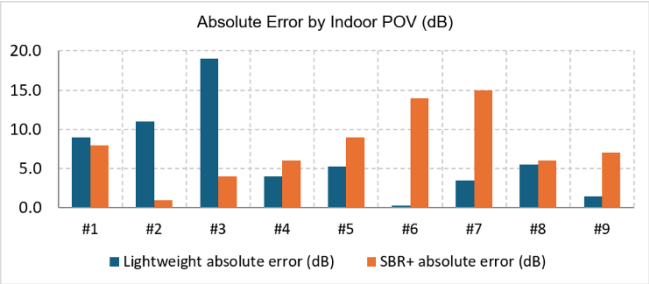

Figure 11. Absolute error at each indoor validation point for the lightweight model and the Ansys HFSS shooting and bouncing rays (SBR+) method is calculated as the absolute difference between the measured median RSRP (reference signal received power) and the corresponding value estimated by each model; smaller errors were found for SBR+ at points #1 to #3, while the lightweight model showed smaller errors at points #4 to #9; the graph of absolute error by indoor point of view (POV) was created by the author using the figures given in Table 5 and Microsoft Excel, version 16.0.

D. Interpretation of results in relation to research questions

Under the Band 66 validation conditions applied in Wayland Hall, the lightweight model matched the measured RSRP with an MAE of 6.57 dB and an RMSE of 8.51 dB, although its accuracy varied substantially by location. The model partially identified the weak-signal locations: points #5 and #9 were among its lowest estimates and were also the two points with the lowest measured median RSRP, but point #8 was predicted to be equally weak as point #9. Compared with SBR+, the lightweight model produced a similar overall error magnitude and smaller pointwise errors at points #4 to #9, whereas SBR+ was closer to the measurements at points #1 to #3 and had the lower maximum absolute error. The largest lightweight-model errors were concentrated at the northern points #1 to #3 and may have been associated with simplified structural representation, uncertain material properties, and propagation mechanisms omitted from the model. Because those factors were not tested separately, their individual effects could not be determined. Overall, specifically under the conditions tested, the lightweight model retained sufficient information to produce an overall error comparable to that of SBR+ while maintaining lower model complexity; however, the results do not demonstrate that it is generally as accurate as or more accurate than SBR+.

E. Limitations and potential applications

The lightweight model focused on distance loss and the losses caused by signals passing through structures. As a result, it did not account for reflection, diffraction, multipath propagation, angle of incidence, phase interference, vertical propagation paths, or smaller architectural details. The model also relied on representative material-loss values selected with reference to prior studies. These values may not fully reflect the properties of the materials used in Wayland Hall. Together, these simplifications may help explain the relatively large prediction errors at points #1 to #3. Because the omitted mechanisms were not introduced and evaluated individually, the study could not determine which simplification contributed most strongly to these errors. The scope of the study was limited to Band 66, north-side incidence, and nine indoor measurement points on the fourth floor of Wayland Hall. The results therefore may not apply directly to other buildings, floors, frequencies, or signal directions. Future studies should evaluate the model in additional buildings and under different incidence directions. Physical effects such as reflection, diffraction, and angle of incidence could then be added individually to determine whether they meaningfully improve prediction accuracy. A closer examination of the propagation paths would also help explain why the SBR+ and lightweight-model results differed substantially at certain locations. Even with these limitations, the lightweight model could serve as a rapid screening tool for identifying areas expected to have relatively weak or strong cellular signals without requiring a complete electromagnetic simulation. For example, it could be used to examine locations that have not yet been measured or to identify areas where additional field measurements may be most useful.

IV. Conclusion

This study assessed the accuracy of indoor cellular signal strength estimation using a simplified propagation model. Measured RSRP values from Wayland Hall were compared with predictions from the lightweight model and normalized results from Ansys HFSS SBR+. For the nine indoor validation points, the lightweight model achieved a mean absolute error (MAE) of 6.57 dB and a root mean square error (RMSE) of 8.51 dB. The corresponding values for SBR+ were 7.78 dB and 8.84 dB, respectively. The lightweight model produced its lowest estimated RSRP at point #5, followed by equal estimates at points #8 and #9. Points #5 and #9 were also the two locations with the lowest measured median RSRP. SBR+ produced smaller pointwise errors at points #1 to #3, whereas the lightweight model produced smaller errors at points #4 to #9. The largest lightweight-model errors occurred at the northern points #1 to #3 and may have been related to simplified geometry, uncertain material-loss values, and propagation mechanisms omitted from the model. Although both models exhibited substantial errors at certain locations, their overall error levels were comparable. Under the tested conditions, these findings indicate that a model based on distance and structure-crossing losses can provide practical estimates of indoor signal distribution without accounting for every propagation effect. The lightweight model was not intended

to replace SBR+ or to demonstrate superior accuracy. Instead, the study aimed to determine the extent to which a limited set of physical mechanisms and a straightforward calculation process could yield useful results. Additional testing is required before broader conclusions can be drawn regarding the model's accuracy or practical applicability. Future research should consider different buildings, frequencies, and signal-incidence directions. Any supplementary physical mechanisms should also be evaluated independently to assess their impact on prediction accuracy.

AI Acknowledgment

The author, Hyundeok Choi, states that Meshy AI was used only for the creation of the initial external geometry as shown in Figure 1; the geometry thus generated was then imported into Free CAD 1.1.1, where it was scaled, corrected, and edited by the author. Meshy AI was not employed for data collection, for the propagation calculations, for the statistical analysis, or for the interpretation of the results.

Acknowledgment

I would like to give a special thanks towards Staff Engineer Mr. Taehyung Kim from the Synopsys Ansys Korea for his support in terms of utilizing Ansys simulation as an electromagnetic simulation to evaluate errors and technical advice on the ray-tracing technique.

References

[1] European Telecommunications Standards Institute. LTE; Evolved Universal Terrestrial Radio Access (E-UTRA); Physical Layer; Measurements (3GPP TS 36.214 Version 16.2.0 Release 16); ETSI TS 136 214 V16.2.0; ETSI: Sophia Antipolis, France, 2021. https://www.etsi.org/deliver/etsi_ts/136200_136299/136214/16.02.00_60/ts_136214v160200p.pdf

[2] Motley, A. J.; Keenan, J. M. P. Personal Communication Radio Coverage in Buildings at 900 MHz and 1700 MHz. *Electron. Lett.* 1988, *24* (12), 763–764. https://doi.org/10.1049/el:19880515

[3] Seidel, S. Y.; Rappaport, T. S. Site-Specific Propagation Prediction for Wireless In-Building Personal Communication System Design. *IEEE Trans. Veh. Technol.* 1994, *43* (4), 879–891. https://doi.org/10.1109/25.330150

[4] Yun, Z.; Iskander, M. F. Ray Tracing for Radio Propagation Modeling: Principles and Applications. *IEEE Access* 2015, *3*, 1089–1100. https://doi.org/10.1109/ACCESS.2015.2453991

[5] International Telecommunication Union. Propagation Data and Prediction Methods for the Planning of Indoor Radiocommunication Systems and Radio Local Area Networks in the Frequency Range from 300 MHz to 450 GHz; Recommendation ITU-R P.1238-13; ITU: Geneva, Switzerland, 2025. https://www.itu.int/rec/R-REC-P.1238-13-202509-I/en

[6] Seidel, S. Y.; Rappaport, T. S. 914 MHz Path Loss Prediction Models for Indoor Wireless Communications in Multifloored Buildings. *IEEE Trans. Antennas Propag.* 1992, *40* (2), 207–217. https://doi.org/10.1109/8.127405

[7] Plets, D.; Joseph, W.; Vanhecke, K.; Tanghe, E.; Martens, L. Simple Indoor Path Loss Prediction Algorithm and Validation in Living Lab Setting. *Wirel. Pers. Commun.* 2013, *68* (3), 535–552. https://doi.org/10.1007/s11277-011-0467-4

[8] Hossain, F.; Geok, T. K.; Rahman, T. A.; Hindia, M. N.; Dimyati, K.; Ahmed, S.; Tso, C. P.; Abd Rahman, N. Z. An Efficient 3-D Ray Tracing Method: Prediction of Indoor Radio Propagation at 28 GHz in 5G Network. *Electronics* 2019, *8* (3), 286. https://doi.org/10.3390/electronics8030286

[9] FreeCAD Project Association AISBL. *FreeCAD*, Version 1.1.1; 2026. https://www.freecad.org/.

[10] Noh, S.-K.; Choi, D.-Y. Propagation Model in Indoor and Outdoor for the LTE Communications. *Int. J. Antennas Propag.* 2019, *2019*, 3134613. https://doi.org/10.1155/2019/3134613

[11] Ansys, Inc. *Near Field Analysis Using Incident Plane Wave in SBR+ Design*; Ansys Electromagnetics Suite 2025 R1, HFSS Help; Ansys, Inc.: Canonsburg, PA, 2025. https://ansyshelp.ansys.com/public/Views/Secured/Electronics/v251/en/Subsystems/HFSS/Content/HFSS/NearFieldAnalysisinSBRPlaneWave.htm.

[12] International Telecommunication Union. *Calculation of Free-Space Attenuation*; Recommendation ITU-R P.525-5; ITU: Geneva, Switzerland, 2024. https://www.itu.int/rec/R-REC-P.525-5-202411-I/en

[13] International Telecommunication Union. *Effects of Building Materials and Structures on Radiowave Propagation in the Range of 1 MHz to 450 GHz*; Recommendation ITU-R P.2040-4; ITU: Geneva, Switzerland, 2025. https://www.itu.int/rec/R-REC-P.2040-4-202509-I/en

[14] Stone, W. C. *Electromagnetic Signal Attenuation in Construction Materials*; NISTIR 6055; National Institute of Standards and Technology: Gaithersburg, MD, 1997. https://doi.org/10.6028/NIST.IR.6055

[15] Ansys, Inc. *HFSS with SBR+*; Ansys Electromagnetics Suite 2025 R2, HFSS Help; Ansys, Inc.: Canonsburg, PA, 2025. https://ansyshelp.ansys.com/public/Views/Secured/Electronics/v252/en/Subsystems/HFSS/Content/HFSS/HFSSSBR.htm.

[16] Ansys, Inc. *Shooting and Bouncing Rays (SBR)*; Ansys Electromagnetics Suite 2025 R1, HFSS Help; Ansys, Inc.: Canonsburg, PA, 2025. https://ansyshelp.ansys.com/public/Views/Secured/Electronics/v251/en/Subsystems/HFSS/Content/HFSS/ShootingAndBouncingRaysSBR.htm

[17] Ansys, Inc. *Selecting a Function for a Plot*; Ansys Electromagnetics Suite 2025 R1, HFSS Help; Ansys, Inc.: Canonsburg, PA, 2025. https://ansyshelp.ansys.com/public/Views/Secured/Electronics/v251/en/Subsystems/HFSS/Content/ReportsandPostProc/SelectingaFunctionforaPlot.htm.

Authors

Hyundeok Choi is a member of Class of 2027 at Wayland Academy. He has interests in mathematics, physics, computational simulation, and game development. He is passionate about utilizing physical models to understand and recreate complex systems in virtual environments. In the future, he hopes to extend his knowledge of interactive digital experiences that combine computation, physics, and creative design and pursue a career in this field.